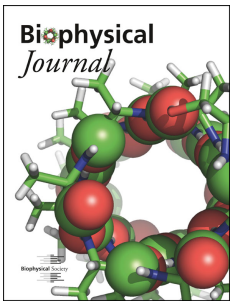
Journal Pre-proof



Front protrusion oscillations indicate positive feedback from protrusion to F-actin network extension in MDA-MB-231 cells, a modeling study

Rainer Marcel Eberhard, Joachim Oskar Rädler, Martin Falcke

PII: S0006-3495(26)00758-7

DOI: https://doi.org/10.1016/j.bpj.2026.11.007

Reference: BPJ 14579

To appear in: *Biophysical Journal*

Received Date: 3 June 2026

Accepted Date: 5 November 2026

Please cite this article as: Eberhard RM, Rädler JO, Falcke M, Front protrusion oscillations indicate positive feedback from protrusion to F-actin network extension in MDA-MB-231 cells, a modeling study, *Biophysical Journal* (2026), doi: https://doi.org/10.1016/j.bpj.2026.11.007.

This is a PDF of an article that has undergone enhancements after acceptance, such as the addition of a cover page and metadata, and formatting for readability. This version will undergo additional copyediting, typesetting and review before it is published in its final form. As such, this version is no longer the Accepted Manuscript, but it is not yet the definitive Version of Record; we are providing this early version to give early visibility of the article. Please note that Elsevier's sharing policy for the Published Journal Article applies to this version, see: https://www.elsevier.com/about/policies-and-standards/sharing#4-published-journal-article. Please also note that, during the production process, errors may be discovered which could affect the content, and all legal disclaimers that apply to the journal pertain.

© 2026 The Author(s). Published by Elsevier Inc. on behalf of Biophysical Society.

Journal Pre-proof

Manuscript submitted to **Biophysical***Journal*
Article

Front protrusion oscillations indicate positive feedback from protrusion to F-actin network extension in MDA-MB-231 cells, a modeling study

Rainer Marcel Eberhard[1], Joachim Oskar Rädler[2], and Martin Falcke[1,3,*]

[1]Max Delbrück Center for Molecular Medicine, Robert-Rössle-Str. 10, 13125 Berlin, Germany
[2]Fakultät für Physik, Ludwig-Maximilians-Universität München, Geschwister-Scholl-Platz 1, 80539 Munich, Germany
[3]Dept. of Physics, Humboldt University, Newtonstr. 15, 12489 Berlin, Germany
[*]Correspondence: martin.falcke@mdc-berlin.de

ABSTRACT Cells moving on one-dimensional lanes exhibit a large variety of coexisting morphodynamic states. MDA-MB-231 cells can show steady or oscillating length while moving, or they can be stationary with steady or oscillating length. Some moving cells exhibit only oscillations of the back protrusion, and some oscillating protrusions at the front and back. The latter state has not been reproduced by any biophysical model, yet. We present a biophysical model for one-dimensional cell motion, which reproduces the variety of motion characteristics observed in experiments. It describes the motion of the body, the front and the back protrusion of a cell, and is based on the force balances at the protrusions edges, protrusion interaction by membrane tension, and the noisy clutch of retrograde flow friction. Integrin signaling controls drag and friction coefficients. Oscillatory morphodynamics arise from stick-slip transitions of the clutch mechanism. Additionally, our model formulates the idea that integrin in nascent adhesions activates Rac, which increases the F-actin network extension rate. This amplification of the polymerization rate at the front protrusion gives rise to moving states with two oscillating protrusions. The increase of the polymerization rate accelerates retrograde flow, making disengagement of the clutch at the front more likely. Therefore, repeated pulling of the back protrusion more significantly affects the motion of the front protrusion. Front oscillations are thus induced by back oscillations as a result of mechanical protrusion interaction. The refined model reproduces all morphodynamic states of one-dimensional cell motion observed in our experiments on MDA-MB-231 cells.

SIGNIFICANCE Morphodynamics of motile cells on 1D lanes may arise from signaling dynamics of small GTPases or the non-linear dynamics of the clutch of retrograde flow. It is a matter of ongoing discussion which concept can explain all of the simultaneously occurring experimental observations like the morphodynamic states and constitutive relations of cell motion. Mechanical models are a promising approach since they can explain all observations except one of the morphodynamic states. Our study closes this gap by introducing local integrin signaling at the leading edge of protrusions into a mechanical model.

INTRODUCTION

Motility is a basic competence of cells. The ability of cells to move is essential in processes such as wound healing, immune response and embryonic development (1). The highly dynamic motion characteristics of these cells exhibit a rich diversity. Cells move at different speeds, come to rest, start moving again or even change directions (2–5). While doing so, they might additionally change their shape. Transitions occur apparently spontaneously without any obvious signaling event, stimulation or perturbation (3).

Many cells moving on flat substrates form a thin sheet-shaped protrusion in the direction of motion (6). Cell motion is driven by actin treadmilling. Actin filaments polymerize at the leading edge of protrusions and push against the cell membrane (6–13). At the same time, the actin network itself moves retrogradely within the protrusion (13, 14), experiencing friction with stationary structures, such as focal adhesions (FA) (15–18). FAs attach the cell to the substrate and stabilize the protrusion (19–24). Retrograde flow friction between FA's and actin network is crucial for migration, as it transmits the protrusion force to the

Journal Pre-proof

substrate, which has been shown by studies on actin network flow (15–18) and measurements of the dynamic force-velocity relation (12). Without a link between actin and the substrate, polymerization could not generate a push force (8).

The friction force of retrograde flow obeys the clutch mechanism (17, 25–32). The relation between friction force and retrograde flow velocity exhibits an increasing force at small velocities up to a critical velocity value beyond which friction force decreases. The force maximum entails stick-slip transitions of sudden speed-up of retrograde flow at the critical velocity due to the decrease of the force resisting motion while the force driving motion is maintained.

Formation of protrusions is controlled by signaling pathways (33–38). An important target of signaling is the RhoGTPase Rac. It activates the WAVE complex, which recruits Arp2/3 to the leading edge membrane, where Arp2/3 initiates the nucleation of new actin filaments branching off existing filaments (23, 39–41). Another essential regulatory element in cell migration is the Rho/ROCK pathway. ROCK - activated by the RhoGTPase RhoA – has several downstream effectors. In addition to increasing myosin II activity (23), it is known to inhibit Rac. In combination with the inhibtion of RhoA by the Rac effector PAK this results in an antagonism of Rac and RhoA reported in many studies and is believed to be a relevant part of the regulation of cell migration (42–44).

Several studies reduced the complexity of cell migration by restricting it to one-dimensional lanes (2–4, 45–50). This restriction revealed surprisingly diverse dynamics of cell motion and shape. While the cells obey the constitutive speed-adhesion relation(49) and the speed-persistence time relation (51), they exhibit at the same time length oscillations both in spread and moving states (4, 49).

Biophysical modeling has the potential to reveal how the processes mentioned above cause the diverse motion characteristics. Mulitple models for 1D motion have been proposed. The ones by Amiri et al. (3) and Sens (46) focus on mechanics. Membrane tension and a clutch mechanism describing the retrograde flow friction mediate protrusion competition, which polarizes the cell. Signaling is not required for polarization in these models. Ron et al. (4) assume in addition to the clutch mechanism an inhibitor of actin polymerization that diffuses and is transported by retrograde flow. Polarization is caused by the concentration gradient of the inhibitor. In all three models, oscillations of the cell length are the result of stick-slip transitions due to the non-linear clutch mechanism. In total, four different states are found: spread steady (SS), spread oscillatory (SO, not in (4)), moving steady (MS) and moving oscillatory (MO). The MO state exhibits oscillation amplitudes at the front which are much smaller than the amplitudes at the back.

Here, we model the behavior of breast epithelial MDA-MB-231 cells on 1D Fibronectin lanes. We have chosen this cell type since it exhibits a large variety of coexisting morphodynamic states (3, 52). Reanalysis of the experimental data from Amiri et al. (3) and Heyn et al. (50) suggests the existence of another state, not yet captured by any of the models. In that state, the cell moves and both protrusions oscillate with comparable amplitudes. Here, we investigate the mechanism causing this morpodynamic state.

We choose the model by Amiri et al. (3) for this study, since it does not only reproduce the four morphodynamic states mentioned above, but also the state fraction and state transition statistics, the speed-adhesion relation and speed-persistence time relation (3). We add to the model the signaling from integrin to Rac and the polymerization rate. When a protrusion builds up, new nascent adhesions form and trigger a signaling cascade activating the Rho-GTPase Rac. This Rac activation by integrin signaling has been reported by a variety of studies (34, 35, 53–58). As mentioned above, Rac promotes actin polymerization. Thus, integrin signaling provides a positive feedback from the protrusion rate to the polymerization rate and with it to the extension rate of the F-actin network. We show how this causes large amplitude oscillations at the front as a result of mechanical protrusion interaction.

METHODS

Our biophysical model for 1D motion of cells is a variation of the model presented in (3). The cell consists of two protrusions of lengths L_f and L_b and the cell body (see Fig. 1). Actin polymerization leads to the extension of the F-actin network pushing the membrane outward in both protrusions. In difference to the previous model, the extension rates $v_{ef,b}$ consist of a constant minimum rate v_e^0 and a part controlled by integrin signaling $v_{ef,b}^+$

$$v_{ef} = v_e^0 + v_{ef}^+, \tag{1}$$

$$v_{eb} = v_e^0 + v_{eb}^+. \tag{2}$$

The signaling-controlled rates $v_{ef,b}^+$ evolve over time obeying

$$\frac{dv_{ef}^+}{dt} = -k v_{ef}^+ + k_v v_f \Theta(v_f), \tag{3}$$

Journal Pre-proof

$$\frac{dv_{eb}^{+}}{dt} = -kv_{eb}^{+} + k_v|v_b|\Theta(-v_b), \tag{4}$$

with the membrane velocities $v_{f,b}$, the rates k and k_v and the Heaviside function $\Theta(x)$.

The signaling-controlled extension rates increase if the membrane moves outward, which is the case for $v_f > 0$ or $v_b < 0$, respectively. In that case, the cell explores new area and nascent adhesions form at a rate proportional to the membrane velocity (23, 54). Nascent adhesions are active signaling complexes that promote actin polymerization by activating Rac. This process is reflected by the second term on the right hand side of Eqs. 3 and 4. After a short lifetime of about 60 s the nascent adhesions either disassemble or grow into larger focal adhesions (23, 35, 54), which do not drive actin polymerization (36, 53). The disassembly rate is independent of the velocity of the membrane (54). We therefore introduced an exponential decay of the signaling-controlled extension rate (first term on the right hand side of Eqs. 3 and 4).

As mentioned above, the decay time of nascent adhesions is about 60 s. The time scale of Rac dynamics is similar (44, 59). Therefore, we take 60 s as the typical time scale of the integrin feedback to the network extension rate. Since the time scale of morphodynamics is longer than 10 min (3), changes in the polymerization rate are fast compared to morphodynamics. We use this time scale separation and assume that the extension rate is always in its stationary state. Eqs. 3 and 4 provide

$$v_{ef}^{+} = \frac{k_v}{k} v_f \Theta(v_f), \tag{5}$$

$$v_{eb}^{+} = \frac{k_v}{k} |v_b| \Theta(-v_b). \tag{6}$$

With $r = k_v/k$ the extension rates yield

$$v_{ef} = v_e^0 + r v_f \Theta(v_f), \tag{7}$$

$$v_{eb} = v_e^0 + r|v_b|\Theta(-v_b). \tag{8}$$

This introduces a dynamic asymmetry of network extension into the model: Instead of constant and equal network extension rates at front and back, the rate at the front can be significantly higher than at the back. For $r = 0$, the model is identical to the model presented in (3) with constant extension rate.

Actin polymerization leads to membrane motion and retrograde flow. Hence, the network extension rate $v_{ef,b}$ is the sum of the edge velocity $v_{f,b}$ and retrograde flow velocity $v_{rf,b}$. We use positive extension rates and retrograde flow velocities, whereas the edge velocities are signed velocities taken in the lab frame of reference. At a given extension rate, retrograde flow is slower when the membrane moves outwards faster. If the membrane is at rest, the retrograde flow is equal to the extension rate. Moving outwards relates to a positive sign at the front and a negative sign at the back. Thus, we obtain:

$$v_{ef} = v_{rf} + v_f, \tag{9}$$

$$v_{eb} = v_{rb} - v_b. \tag{10}$$

We neglect the force dependence of the network extension rate used in Amiri et al. (3) since they showed that network extension rate changes turned out to be less than 8% which is too small to be relevant.

The force pushing the membrane protrusion at the leading edge is equal to the force driving retrograde flow there. Thus, force balances at the edges of the protrusions comprise drag forces ($\zeta v_{f,b}$) resisting membrane motion and elastic forces ($E(L_{f,b} - L_0)$) due to cell stretching, and the force required to drive retrograde flow at the leading edge which is equal to the flow friction force ($\kappa_{f,b} v_{rf,b}$ with the friction coefficients $\kappa_{f,b}$). The use of elastic forces has been supported by experiments on length changes at Fibronectin density steps (3). They can be membrane tension or other length-dependent cytoskeletal forces. The elastic forces act on the cell body and determine its velocity v_c:

$$\kappa_f v_{rf} - E(L_f - L_0) - \zeta v_f = 0, \tag{11}$$

$$E(L_f - L_0) - E(L_b - L_0) - b\zeta v_c = 0, \tag{12}$$

$$-\kappa_b v_{rb} + E(L_b - L_0) - \zeta v_b = 0. \tag{13}$$

The relative contribution of the cell body to cell drag is determined by the parameter b.

The protrusion lengths change due to velocity differences between the edges and the cell body:

$$\frac{dL_f}{dt} = v_f - v_c, \tag{14}$$

$$\frac{dL_b}{dt} = v_c - v_b. \tag{15}$$

The friction between retrogradely flowing F-actin and intracellular structures obeys the clutch mechanism, as has been reported in a variety of studies (17, 25–27, 29–32, 60–63). Retrograde flow friction is modeled using a dynamic friction coefficient κ determined by the number of bonds between the actin network and focal adhesions. We use the bond formation and dissociation rates established by Craig et al. (32). The bond dynamics implement the clutch mechanism: A large friction coefficient means that many bonds connect F-actin and the stationary structures - the clutch is engaged. Smaller values mean that bonds broke, the clutch is disengaged. The dissociation rate κ_{off} increases as retrograde flow speeds up. It depends exponentially on the retrograde flow velocity (32, 64, 65). This motivates the following dynamics (32):

$$\frac{d\kappa_{f,b}}{dt} = k_{on}(\kappa^{lim} - (\kappa_{f,b} - \kappa_0)) - k^0_{off} e^{\frac{|v_{rf,b}|}{v_{slip}}} (\kappa_{f,b} - \kappa_0) + \eta_{f,b}(t). \tag{16}$$

κ_0 is the minimum and κ^{lim} the maximum value of κ, k_{on} is the binding rate, $k_{off} = k^0_{off} e^{\frac{|v_{rf,b}|}{v_{slip}}}$ the unbinding rate with the slip velocity v_{slip}. Retrograde flow friction is present in both protrusions. The larger the friction, the slower the actin flows backwards and the faster the membrane is pushed outward (see Eqs. 9 and 10). Thus, the cell moves in direction of higher retrograde flow friction as a result of mechanical protrusion competition. We assume that random formation and dissociation of bonds is the major source of noise in the dynamics of the friction coefficient. Therefore, we add the noise terms $\eta_{f,b}(t)$ to the bond dynamics.

Gaussian white noise $\eta_{f,b}$ is added with a noise amplitude determined by (3),

$$\langle \eta_{f,b}(t) \rangle = 0 \tag{17}$$

$$\langle \eta_{f,b}(t)\eta_{f,b}(t') \rangle = \frac{k_{on}(\kappa^{lim} - \kappa_{f,b}) + k^0_{off} e^{\frac{|v_{rf,b}|}{v_{slip}}} \kappa_{f,b}}{\alpha \kappa^{lim}_{b,f}} \delta(t - t'). \tag{18}$$

Eq. 18 is discussed in more detail in section S3. The parameter α scales the noise amplitude and is defined in this section.

The density of adhesion-related stationary structures and strength of adhesion is controlled by the substrate density of the integrin ligand Fibronectin (FN) (20–22). Hence, κ^{lim} and the drag coefficient ζ depend on the ligand substrate density B in a Hill-type relation (3):

$$\kappa^{lim} = \kappa_0 + \frac{\kappa^{max} B^{n_\kappa}}{K^{n_\kappa}_\kappa + B^{n_\kappa}} \tag{19}$$

$$\zeta^{lim} = \zeta_0 + \frac{\zeta^{max} B^{n_\zeta}}{K^{n_\zeta}_\zeta + B^{n_\zeta}}. \tag{20}$$

κ^{max} and ζ^{max} are the upper limits of the friction and drag coefficients at saturating ligand density, respectively. $K_{\zeta,\kappa}$ and $n_{\zeta,\kappa}$ are the Hill parameters.

The model is strictly symmetric with regard to parameter values. Polarization is caused by mechanical protrusion competition. Once, polarization is established, the network extension rates can significantly differ between front and back. As the cell changes direction, the protrusions swap roles. Hence, we observe a dynamic asymmetry with regard to network extension rates.

To obtain simulated cell trajectories, we numerically solve the 4-component dynamical system given by Eqs. 14-16. The noise-free system exhibits stationary states and limit cycles, which are the morphodynamic states of cell motion. We use parameter set 1 in Table S1 for the simulations in Figs. 2-4. This set of parameter values has been obtained by fitting the original model to a large variety of experimental data in Amiri et al. (3). Fig. 5 uses parameter set 2 from Table S1. It is very similar but not identical to set 1 and has been obtained by fitting state transition statistics with the current model.

RESULTS

Membrane velocity dependent polymerization rates lead to an additional morphodynamic state

Our noise-free model exhibits five distinct dynamic states of cell motion, four of which were already found using the previous model (SS, SO, MS, MO) (3). Cells in the spread steady (SS) state do not move at all, cells in the spread oscillatory (SO) state are at rest but oscillate in length. Moving cells with fixed length are in the moving steady state (MS). The moving oscillatory state (MO) is characterized by an oscillating back protrusion. Here, we find another state, where the cell moves but in contrast to the MO state, both protrusions oscillate. Fig. 2(E-I) shows example trajectories for each of the five states.

Journal Pre-proof

Fig. 2(A-D) displays bifurcation diagrams, illustrating the morphodynamic states through the values of the friction coefficient κ for different values of the parameter r. The model is equivalent to the model presented in (3) for $r = 0$. In each case, the SS state is the only stable state at very small B. It becomes unstable at the *branch point (BP)* and the MS state emerges. At the *Hopf bifurcation points* oscillations start and the SS and MS states change into SO and MO, respectively. For small r (Fig. 2(A, B)) the oscillations of κ_f have small amplitudes. At larger r (Fig. 2(C, D)) the oscillations become significant and another state with both protrusions oscillating is observed. Fig. S1 shows a comparison of the three moving states. Whereas all quantities are constant over time in the MS state, oscillations are observed in the other two states. However, oscillations at the front have very small amplitudes in the MO state and only become significant for the MO2 state.

Moving states are excitable by noise in the bond dynamics

The coexistence of all morphodynamic states of MDA-MB-231 cells has been shown in experiments in Amiri et al. (3). In the deterministic model, we do not observe multistability between all states. Particularly, we lack the coexistence between the two spread states (SS, SO) and the three moving states (MS, MO, MO2). However, Amiri et al. (3) showed that the steady states are excitable by noise in the bond dynamics leading to noisy oscillations, which explains the coexistence of the steady and oscillatory states. We show that the moving states are excitable and can transition into a noisy MO2 state.

For that matter, we simulated cell trajectories initially in one of the three moving states in the noise-free system (Fig. 3(E, G, I)). After 5 h, we turned on the noise in the bond dynamics (indicated by the vertical dashed line in Fig. 3(E, G, I)). Each cell transitions into the MO2 state with noisy oscillations at the front and back protrusion. This state is very similar to MO2 states observed in experimental data (Fig. 3(A) (3) and (B) (50)). As each moving state can transition into the MO2 state, its existence is possible in a wide range of ligand densities B.

Fig. 3(B, D, F, H, J) shows the membrane velocities $v_{f,b}$ over time for the respective trajectory. Sharp positive peaks for the back velocity and sharp negative peaks for the front velocity indicate a protrusion collapse, i.e. fast reduction of length. In the noisy MO2 state, we observe repeated protrusion collapses at the front and back in experiment and simulations. In contrast to that, in the deterministic MO state the front velocity is almost constant, while in the deterministic MO2 state it oscillates but no sharp peaks, i.e. collapsing protrusions, are observed. The experimental records in Fig. 3(B, D) are more similar to the noisy parts of the simulations than to the deterministic parts.

Oscillations at the back induce oscillations at the front as a result of protrusion competition

Excitability and oscillations are a result of coupled feedback loops in many biological systems (3, 66). In our model, we have a positive and negative feedback loop with regard to the evolution of the friction coefficient. Increasing κ leads to slower retrograde flow and hence decreasing dissociation rate (see Eq. 16), stabilizing bonds and κ. On the other hand, decreasing retrograde flow also leads to increased membrane velocity. The protrusion grows, and the elastic force increases, which in turn resists the growing protrusion. The membrane slows down and retrograde flow speeds up, leading to a higher dissociation rate and therefore decreasing κ. Depending on the model parameters and the ligand density B, the feedback loops can cooperate to induce stick-slip oscillations as observed in the SO and MO state (3). But how do the oscillations at the front protrusion in the MO2 state arise?

In the model presented in this work, we added that the actin network extension rate depends on the membrane velocity in a way, that the rate is increased if the membrane moves outward. Hence, in moving states, the extension rate at the front is always larger than in the symmetric model ($r = 0$) as v_{ef}^{+} is added to the minimum extension rate v_e^0 (see Eq. 1). Since the extension rate is the sum of the membrane and retrograde flow velocities (Eq. 9), the retrograde flow speeds up as r increases for a given membrane velocity (see Eqs. 7 and 9). Consequently, the dissociation rate is higher and κ smaller. This can be clearly observed in the bifurcation diagrams in Fig. 3(A-D).

In Fig. 4(A,B) we compare the MO2 state for $r = 0.7$ and the MO state for $r = 0$ at the same ligand density B = 80 ng/cm^2. The amplitude of oscillations of the back friction coefficient are slightly larger in the MO2 state and the friction coefficient at the front is significantly smaller than in the MO state (Fig. 4(A, B second row)). Therefore, retrograde flow is faster in the MO2 state while the membranes move at similar speeds (Fig. 4(A, B third and forth row)). As a result, the protrusion competition is much more "competitive" in the MO2 state. During each oscillation, when κ_b reaches its maximum, the back protrusion pulls on the front. In the MO state, where differences between the maximum at the back and κ_f are large, this pulling has little effect on the front protrusion, retrograde flow velocity and membrane velocity remain basically constant (Fig. 4(A third and forth row)). If friction coefficients are closer like in the MO2 state, the back pulls strongly on the front and significantly affects its motion, leading to oscillations of the front membrane velocity (Fig. 4(B bottom row).

In a way, we can view MO2 oscillations as a repeated perturbation of front motion by back oscillations. In Fig. 4(C, D), we perturbed a cell in the MS state by increasing the back friction coefficient at one point in time. If the perturbation is weak

(Fig. 4C), it only slightly affects the front protrusion. Retrograde flow velocity and membrane velocity stay almost constant (Fig. 4(C third and fourth row)). Although a back protrusion is forming, the effect on the leading edge motion is vanishingly small (Fig. 4(C first row)). A larger perturbation (Fig. 4(D)) reaching almost the friction coefficient at the front leads to a significant drop in the friction coefficient at the front, which entails an increased retrograde flow and a slowing of the leading edge (Fig. 4(D second to last row)). The cell almost stalls and then keeps moving in the initial direction (Fig. 4(D first row)). The MO2 state is similar to repeated stronger perturbations, whereas the MO state is similar to repeated weak perturbations.

Biophysical model reproduces state distribution and state transition statistics of MDA-MB-231 cells

We analyzed the single cell trajectories of MDA-MB-231 cells taken from Amiri et al. (3) with regard to the cell states presented above, following a similar approach as therein. At first, state change points are determined using an iterative method based on cumulative sum (CUSUM) statistics. This algorithm detects time points where the trend of motion changes and thus segments the trajectory. To each segment, we can assign a morhphodynamic state. A cell is considered to be in a specific state only if it shows consistent behavior for at least 1 h. Consequently, state change points have to be at least 1 h apart.

To assign a state to a segment, we use three metrics, two of which we adopt from Amiri et al. First, we distinguish spread and moving states using a velocity threshold ($0.002 \mu m s^{-1}$). Second, we distinguish steady and oscillatory states using an oscillation index, based on fluctuations in cell length and the nucleus motion (see supplemental section S2 for details). If this index is above a threshold, the cell is classified as oscillatory. Third, based on that oscillation index, we introduce a second oscillation index using fluctuations of the front protrusion length to distinguish between MO and MO2 (see also supplemental section S2).

We applied this procedure to the experimental data and determined the fraction of time spent in each state, as well as the probability of transitions between states (Fig. 5(B, C)). We simulated 1000 cell trajectories with a length of 24 h each for each set of parameters tested within the fit procedure. We applied the same procedure to the simulated data as we applied to the experimental data to analyze state statistics. Simulations account for cell variability by randomly sampling parameter values from a range of ±5% around the value given in set 2 of Table S1. This parameter set was found by varying the values of parameter set 1, which was taken from Amiri et al. (3) until we reach good agreement between simulation and experiment (Fig. 5).

What can be concluded from this type of analysis has been discussed in detail in Amiri et al. (3). We can conclude the types of observed states based on their phenomenological definition, the types of observed transitions between states and their statistics from this comparison between experimental and simulated trajectories. We cannot conclude bifurcation diagrams from this analysis since the detection of a state does not necessarily indicate its stability (see section S2).

Additionally, small changes in model parameter values may entail qualitative changes of the bifurcation diagram (3) as we also find here. There are three differences between the bifurcation diagram belonging to parameter set 1 Fig. 2 and set 2 Fig. 5(A). First, we find two *Hopf bifurcations* on the branches representing the moving states. At the first one, oscillations arise (MO) and the MS state becomes unstable. With rising FN density, front oscillations increase leading to the existence of the MO2 state. At the second *Hopf bifurcation* the MS state becomes stable again, such that we have a bistability of MS and MO2. The second alteration is the existence of a *limit point*, where a stable and an unstable limit cycle emerge. The latter terminates at the second *Hopf bifurcation*. The last and most significant difference to the bifurcation diagrams above is the lack of the *Hopf bifurcation* on the SS branch, sucht that there is no stable SO state. Since the SS state is excitable by noise similar to what we have shown for the moving states above (3), we still expect to observe SO states in our cell trajectories. However, the SS state is only stable at low FN densities. This poses the question how we still observe both spread states over a wide range of FN densities as well as transitions between all states.

To answer this, we first have to notice, that the classification algorithm described above solely relies on the positions of nucleus and front and back membrane. It does not take into account the mathematical state of the dynamical system. For experimental data the mathematical state is unknown and for comparability, we used the same method to detect morphodynamic states in simulation data. Thus, the algorithm might detect a specific state, although the dynamical system is not in the corresponding mathematical state. We can think of several possibilities explaining the observed transitions: 1) We use a velocity threshold to distinguish spread and moving states. If a cell moves very slowly, the corresponding segment will be classified as spread (MS becomes SS, MO/MO2 become SO). 2) Back pulling events can lead to the nucleus stalling (see Fig. 4(D)). If this phase it sufficiently long it might be classified as a spread state. 3) Direction reversals are not always sharp. This can lead to a segmentation into "moving up" → "spread" → "moving down", instead of switching from moving up to down directly. Mathematically, this could mean, that the system is transiently close to the unstable spread state during the transition between the two stable moving states. 4) Frequent direction reversals over a short time without net motion resemble the SO state and thus might be classified as such. In supplemental Fig. S2, we collected a selection of trajectories displaying these behaviors.

In summary, our model reproduces the state distribution and state transition statistics of MDA-MB-231 cells. The states are

Journal Pre-proof

defined using velocity and oscillation metrics based on the temporal positions of nucleus and front and back membrane rather than the underlying mathematical state.

DISCUSSION

Cells moving in one dimension exhibit rich dynamics of motion and shape. Several morphodynamic states coexist and spontaneously transition into each other. We distinguish spread and moving states and states with oscillatory or steady length. Additionally, cells obey the constitutive speed-adhesion and speed-persistence time relation (49, 51). Cells obey the constitutive relations while exhibiting morphodynmaics. Models that account for this ubiquitousness can explain the experimentally observed morphodynamic state of moving cells in which the back protrusion oscillates but not states in which the front protrusion also does (state MO2) (3, 49, 50). In this work, we close this gap by presenting a variation of the model by Amiri et al. (3), which also exhibits the front oscillations.

We complement the model by proposing that a dynamic feedback from the protrusion velocity to the polymerization rate mediated by integrin signaling to Rac, which has been used also by Welf et al. (58), causes front oscillations. It suggests, that nascent adhesions form as the protrusion extends, integrin receptors bind to their ligands on the substrate and promote actin polymerization by activation of Rac (23, 34, 35, 53, 54). In its net effect, this is a local self-amplification of the polymerization rate. The retrograde flow in cells with this local positive feedback is faster than in cells without it moving at the same velocity. The cells with this feedback are more likely to disengage the clutch of retrograde flow in the front protrusion. Therefore, the front protrusion responds more strongly to the pulling of the back protrusion. That causes the front oscillations.

We assume that the local positive feedback from protrusion to polymerization is required for the dynamic state MO2. Different molecular realizations of this feedback are reported in several studies (35, 55, 57, 67, 68). Rac GEFs like DOCK180 or β-PIX are recruited to the leading edge by paxillin phosphorylation mediated interaction with the p130CAS-Crk complex and the apator GIT1, respectively. The inhibition of these pathways at any point are candidates for perturbation experiments, which we expect to result in a decrease of front oscillations. Other models including the clutch mechanism but not the local protrusion amplification exhibit the states SS, SO, MS and MO but not MO2 (4, 46). We also tested alternative hypotheses in our search for the mechanism generating the MO2 state. Asymmetric protrusions with regard to parameter values was an obvious candidate. Using different fixed network extension rates at front and back makes the MS state the only stable state at small ligand densities instead of SS. The same holds for different κ^{max} or ζ^{max} at front and back. This is interesting in that we observe resting and moving cells at small ligand densities in experiments (3). Protrusion asymmetry accounts for this experimental observation, but it does not generate any additional morphodynamic state.

We also investigated a dependence of the polymerization rate on other quantities. But neither an increase of polymerization rate with increasing friction coefficients or friction forces nor a reduction upon faster retrograde flow leads to the emergence of the MO2 state. These approaches involve negative feedback loops which in the end suppress oscillations. For example, the rise of the polymerization rate upon increased κ entails also faster retrograde flow, which increases the dissociation rate and reduces κ again. Reduced κ leads to decreased polymerization rate, which compensates the initial increase. This type of a negative feedback loop is avoided in the mechanism suggested in this work. In summary, all the other tested mechanisms without the local positive feedback from protrusion to polymerization did not cause MO2.

Welf et al. included the positive feedback from protrusion to polymerization mediated by Rac into their model by a slightly different mathematical realization, i.e. by using dynamic Rac concentration (58). A direct comparison of results is difficult, since our study and Welf et al. focus on different aspects. Interestingly, Welf et al. suggest to study situations where "cessation of protrusion, brought about by increased retrograde flow, is accompanied by failure of the clutch" to study mechanisms involving speed up of retrograde and the clutch (58). Here we see that the suggested direction of thinking provided valuable insight into oscillation mechanisms.

Our model describes the mechanical interaction between protrusions and shows how that interaction leads to morphodynamics (3, 49, 50). It does not describe the generation of protrusions, which is controlled by signaling involving small GTPases (69–72). Cells exhibit protrusions at both ends most of the time in our experiments (see Fig. 3A, C and (3)). The model proposes that polarization is the result of mechanical protrusion competition. The clutch of retrograde flow is the core mechanism of this competition. It is disengaged when retorgrade flow is fast and engaged when it is slow. Retrograde flow in the back protrusion is the sum of network extension rate and cell velocity and, therefore, it is fast. Retrograde flow in the front protrusion is the difference of network extension rate and cell velocity and, therefore, it is much slower than in the back. The clutch in the front is engaged, the one in the back is disengaged (or less engaged). That polarizes the cell.

The oscillation mechanism supports the idea that protrusion interaction across the entire length of the cell is mediated mechanically, i.e. by membrane tension. Alternative ideas imply the diffusion or advection of a polymerization inhibitor (4) or inhibitor of protrusion formation (discussed in Mori et al. (73), Holmes et al. (42)) across the entire cell as means of protrusion competition. We observed MDA-MB-231 cells with lengths exceeding 50 µm in previous works (3, 49, 50). In ongoing research

Journal Pre-proof

we see RPE cells exhibiting protrusion competition with a length of more than 300 µm (74). That renders protrusion competition by signaling less likely since diffusion time scales are much longer than morphodynamic time scales with these cell lengths.

We investigated only MDA-MB-231 cells and no other cell types in this study. Hence, we do not know whether our results apply to the motion of other cell types. However, our modelling approach does not involve assumptions applying to MDA-MB-231 cells only. Both the clutch of retrograde flow and Rac signalling have been observed in a variety of cells. Hence, it is possible that different parameter sets of our model describe the behavior of different cell types.

CONCLUSIONS

We presented an advance of the protrusion competition model introduced by Amiri et al. (3). This model captures the large variability of morphodynamic states of cell motion with now five distinct states: spread steady (SS), spread oscillatory (SO), moving steady (MS) and two moving oscillatory (MO,MO2) states with either only the back or both protrusions oscillating. Local amplification of the polymerization rate due to faster protrusion rates causes the morphodynamic state with both protrusions oscillating (MO2), such that the refined model offers explanations for the full variety of morphodynamic states and their multistability. Since the model also exhibits the constitutive speed-adhesion and speed-peristence time relation (3, 49), it offers a biophysical explanation for the concomitant observations in cell motility.

DATA AVAILABILITY

All code for simulations and analysis can be found in the supplementing zenodo repository. Experimental data analyzed within this work is already published along with Amiri et al. (3) and Heyn et al. (50).

AUTHOR CONTRIBUTIONS

RME developed and simulated the model, analyzed data, JOR supervised experimental work and provided experimental data, MF supervised theoretical work, RME, MF wrote the article.

DECLARATION OF INTERESTS

The authors declare no competing interests.

ACKNOWLEDGMENTS

This work was funded by DFG grant Fa350/19-1 to M.F.

SUPPLEMENTARY MATERIAL

An online supplement to this article can be found by visiting BJ Online at http://www.biophysj.org.

SUPPORTING CITATIONS

References (75–83) appear in the Supporting Material.

REFERENCES

1. Pollard, T. D., and G. G. Borisy, 2003. Cellular Motility Driven by Assembly and Disassembly of Actin Filaments. *Cell* 112:453–465.

2. Hennig, K., I. Wang, P. Moreau, L. Valon, S. DeBeco, M. Coppey, Y. A. Miroshnikova, C. Albiges-Rizo, C. Favard, R. Voituriez, and M. Balland, 2020. Stick-slip dynamics of cell adhesion triggers spontaneous symmetry breaking and directional migration of mesenchymal cells on one-dimensional lines. *Sci. Adv.* 6:eaau5670.

3. Amiri, B., J. C. J. Heyn, C. Schreiber, J. O. Rädler, and M. Falcke, 2023. On multistability and constitutive relations of cell motion on fibronectin lanes. *Biophys. J.* 122:753–766.

4. Ron, J. E., P. Monzo, N. C. Gauthier, R. Voituriez, and N. S. Gov, 2020. One-dimensional cell motility patterns. *Phys. Rev. Res.* 2:033237.

Journal Pre-proof

5. Maiuri, P., E. Terriac, P. Paul-Gilloteaux, T. Vignaud, K. McNally, J. Onuffer, K. Thorn, P. A. Nguyen, N. Georgoulia, D. Soong, A. Jayo, N. Beil, J. Beneke, J. C. Hong Lim, C. Pei-Ying Sim, Y.-S. Chu, A. Jiménez-Dalmaroni, J.-F. Joanny, J.-P. Thiery, H. Erfle, M. Parsons, T. J. Mitchison, W. A. Lim, A.-M. Lennon-Duménil, M. Piel, and M. Théry, 2012. The first World Cell Race. *Curr. Biol.* 22:R673–R675. http://www.sciencedirect.com/science/article/pii/S0960982212008779.

6. Abercrombie, M., 1980. The Croonian Lecture, 1978 - The crawling movement of metazoan cells. *Proc. R. Soc. Lond. B Biol. Sci.* 207:129–147. https://royalsocietypublishing.org/doi/abs/10.1098/rspb.1980.0017.

7. Small, J. V., T. Stradal, E. Vignal, and K. Rottner, 2002. The lamellipodium: where motility begins. *Trends Cell Biol.* 12:112 – 120.

8. Pollard, T., 2003. The cytoskeleton, cellular motility and the reductionist agenda. *Nature* 422:741–745.

9. Dimchev, G., B. Amiri, F. Fäßler, M. Falcke, and F. K. Schur, 2021. Computational toolbox for ultrastructural quantitative analysis of filament networks in cryo-ET data. *J. Struct. Biol.* 213:107808. https://www.sciencedirect.com/science/article/pii/S1047847721001131.

10. Prass, M., K. Jacobson, A. Mogilner, and M. Radmacher, 2006. Direct measurement of the lamellipodial protrusive force in a migrating cell. *J. Cell Biol.* 174:767–772.

11. Heinemann, F., H. Doschke, and M. Radmacher, 2011. Keratocyte Lamellipodial Protrusion Is Characterized by a Concave Force-Velocity Relation. *Biophys. J.* 100:1420 – 1427.

12. Zimmermann, J., C. Brunner, M. Enculescu, M. Goegler, A. Ehrlicher, J. Käs, and M. Falcke, 2012. Actin Filament Elasticity and Retrograde Flow Shape the Force-Velocity Relation of Motile Cells. *Biophys. J.* 102:287 – 295.

13. Svitkina, T. M., A. B. Verkhovsky, K. M. McQuade, and G. G. Borisy, 1997. Analysis of the Actin-Myosin II System in Fish Epidermal Keratocytes: Mechanism of Cell Body Translocation. *J. Cell Biol.* 139:397 – 415.

14. Vallotton, P., G. Danuser, S. Bohnet, J.-J. Meister, and A. B. Verkhovsky, 2005. Tracking Retrograde Flow in Keratocytes: News from the Front. *Mol. Biol. Cell* 16:1223–1231.

15. Alexandrova, A. Y., K. Arnold, S. Schaub, J. M. Vasiliev, J.-J. Meister, A. D. Bershadsky, and A. B. Verkhovsky, 2008. Comparative Dynamics of Retrograde Actin Flow and Focal Adhesions: Formation of Nascent Adhesions Triggers Transition from Fast to Slow Flow. *PLoS One* 3:e3234.

16. Fournier, M. F., R. Sauser, D. Ambrosi, J.-J. Meister, and A. B. Verkhovsky, 2010. Force transmission in migrating cells. *J. Cell Biol.* 188:287–297.

17. Jurado, C., J. R. Haserick, and J. Lee, 2005. Slipping or Gripping? Fluorescent Speckle Microscopy in Fish Keratocytes Reveals Two Different Mechanisms for Generating a Retrograde Flow of Actin. *Mol. Biol. Cell* 16:507–518.

18. Renkawitz, J., K. Schumann, M. Weber, T. Lämmermann, H. Pflicke, M. Piel, J. Polleux, J. P. Spatz, and M. Sixt, 2009. Adaptive force transmission in amoeboid cell migration. *Nat. Cell Biol.* 11:1438–1443.

19. Sheetz, M. P., D. P. Felsenfeld, and C. G. Galbraith, 1998. Cell migration: regulation of force on extracellular-matrix-integrin complexes. *Trends Cell Biol.* 8:51 – 54.

20. Huttenlocher, A., M. H. Ginsberg, and A. F. Horwitz, 1996. Modulation of cell migration by integrin-mediated cytoskeletal linkages and ligand-binding affinity. *J. Cell Biol.* 134:1551–1562. https://doi.org/10.1083/jcb.134.6.1551.

21. Palecek, S. S., J. C. Loftus, M. H. Ginsberg, D. A. Lauffenburger, and A. F. Horwitz, 1997. Integrin-ligand binding properties govern cell migration speed through cell-substratum adhesiveness. *Nature* 385:537–540.

22. Vicente-Manzanares, M., C. K. Choi, and A. R. Horwitz, 2009. Integrins in cell migration - the actin connection. *J. Cell Sci.* 122:199–206.

23. Parsons, J. T., A. R. Horwitz, and M. A. Schwartz, 2010. Cell adhesion: integrating cytoskeletal dynamics and cellular tension. *Nat. Rev. Mol. Cell Biol.* 11:633–643.

Journal Pre-proof

24. Burridge, K., and C. Guilluy, 2016. Focal adhesions, stress fibers and mechanical tension. *Exp. Cell Res.* 343:14 – 20.

25. Mitchison, T., and M. Kirschner, 1988. Cytoskeletal dynamics and nerve growth. *Neuron* 1:761 – 772.

26. Suter, D. M., and P. Forscher, 1998. An emerging link between cytoskeletal dynamics and cell adhesion molecules in growth cone guidance. *Curr. Opin. Neurobiol.* 8:106–116.

27. Suter, D. M., and P. Forscher, 2000. Substrate–cytoskeletal coupling as a mechanism for the regulation of growth cone motility and guidance. *J. Neurobiol.* 44:97–113.

28. Hu, K., L. Ji, K. T. Applegate, G. Danuser, and C. M. Waterman-Storer, 2007. Differential transmission of actin motion within focal adhesions. *Science* 315:111–115. <GotoISI>://WOS:000243259100049.

29. Gardel, M. L., B. Sabass, L. Ji, G. Danuser, U. S. Schwarz, and C. M. Waterman, 2008. Traction stress in focal adhesions correlates biphasically with actin retrograde flow speed. *J. Cell Biol.* 183:999–1005.

30. Aratyn-Schaus, Y., and M. L. Gardel, 2010. Transient Frictional Slip between Integrin and the ECM in Focal Adhesions under Myosin II Tension. *Curr. Biol.* 20:1145–1153.

31. Li, Y., P. Bhimalapuram, and A. R. Dinner, 2010. Model for how retrograde actin flow regulates adhesion traction stresses. *J. Phys.: Condens. Matter* 22:194113.

32. Craig, E. M., J. Stricker, M. Gardel, and A. Mogilner, 2015. Model for adhesion clutch explains biphasic relationship between actin flow and traction at the cell leading edge. *Phys. Biol.* 12.

33. Ridley, A. J., 2001. Rho GTPases and cell migration. *J. Cell Sci.* 114:2713–2722.

34. Ridley, A. J., M. A. Schwartz, K. Burridge, R. A. Firtel, M. H. Ginsberg, G. Borisy, J. T. Parsons, and A. R. Horwitz, 2003. Cell migration: integrating signals from front to back. *Science* 302:1704–1709.

35. Vicente-Manzanares, M., and A. R. Horwitz, 2011. Adhesion dynamics at a glance. *J. Cell Sci.* 124:3923–3927.

36. Devreotes, P., and A. R. Horwitz, 2015. Signaling networks that regulate cell migration. *Cold Spring Harb. Perspect. Biol.* 7:a005959.

37. Harburger, D. S., and D. A. Calderwood, 2009. Integrin signalling at a glance. *J. Cell Sci.* 122:159–163.

38. Warner, H., B. J. Wilson, and P. T. Caswell, 2019. Control of adhesion and protrusion in cell migration by Rho GTPases. *Curr. Opin. Cell Biol.* 56:64–70.

39. Petrie, R. J., A. D. Doyle, and K. M. Yamada, 2009. Random versus directionally persistent cell migration. *Nat. Rev. Mol. Cell Biol.* 10:538–549.

40. de Beco, S., K. Vaidžiulytė, J. Manzi, F. Dalier, F. Di Federico, G. Cornilleau, M. Dahan, and M. Coppey, 2018. Optogenetic dissection of Rac1 and Cdc42 gradient shaping. *Nat. Commun.* 9:4816.

41. Yang, H. W., S. R. Collins, and T. Meyer, 2016. Locally excitable Cdc42 signals steer cells during chemotaxis. *Nat. Cell Biol.* 18:191–201.

42. Holmes, W. R., J. Park, A. Levchenko, and L. Edelstein-Keshet, 2017. A mathematical model coupling polarity signaling to cell adhesion explains diverse cell migration patterns. *PLoS Comput. Biol.* 13:e1005524.

43. Bolado-Carrancio, A., O. S. Rukhlenko, E. Nikonova, M. A. Tsyganov, A. Wheeler, A. Garcia-Munoz, W. Kolch, A. von Kriegsheim, and B. N. Kholodenko, 2020. Periodic propagating waves coordinate RhoGTPase network dynamics at the leading and trailing edges during cell migration. *eLife* 9:e58165.

44. Machacek, M., L. Hodgson, C. Welch, H. Elliott, O. Pertz, P. Nalbant, A. Abell, G. L. Johnson, K. M. Hahn, and G. Danuser, 2009. Coordination of Rho GTPase activities during cell protrusion. *Nature* 461:99–103.

45. Guetta-Terrier, C., P. Monzo, J. Zhu, H. Long, L. Venkatraman, Y. Zhou, P. Wang, S. Y. Chew, A. Mogilner, B. Ladoux, and N. C. Gauthier, 2015. Protrusive waves guide 3D cell migration along nanofibers. *J. Cell Biol.* 211:683–701. https://doi.org/10.1083/jcb.201501106.

Journal Pre-proof

46. Sens, P., 2020. Stick–slip model for actin-driven cell protrusions, cell polarization, and crawling. *Proc. Natl. Acad. Sci. U.S.A.* 117:24670–24678.

47. Jain, S., V. M. L. Cachoux, G. H. N. S. Narayana, S. de Beco, J. D'Alessandro, V. Cellerin, T. Chen, M. L. Heuzé, P. Marcq, R.-M. Mège, A. J. Kabla, C. T. Lim, and B. Ladoux, 2020. The role of single-cell mechanical behaviour and polarity in driving collective cell migration. *Nat. Phys.* 16:802–809. https://doi.org/10.1038/s41567-020-0875-z.

48. Sheets, K., S. Wunsch, C. Ng, and A. S. Nain, 2013. Shape-dependent cell migration and focal adhesion organization on suspended and aligned nanofiber scaffolds. *Acta Biomater.* 9:7169–7177.

49. Schreiber, C., B. Amiri, J. C. J. Heyn, J. O. Rädler, and M. Falcke, 2021. On the adhesion–velocity relation and length adaptation of motile cells on stepped fibronectin lanes. *Proc. Natl. Acad. Sci. U.S.A.* 118. https://www.pnas.org/content/118/4/e2009959118.

50. Heyn, J. C., M. Atienza Juanatey, M. Falcke, and J. O. Rädler, 2025. Cell-mechanical parameter estimation from 1D cell trajectories using simulation-based inference. *PLoS One* 20:e0310669.

51. Maiuri, P., J.-F. Rupprecht, S. Wieser, V. Ruprecht, O. Bénichou, N. Carpi, M. Coppey, S. D. Beco, N. Gov, C.-P. Heisenberg, C. L. Crespo, F. Lautenschlaeger, M. L. Berre, A.-M. Lennon-Dumenil, M. Raab, H.-R. Thiam, M. Piel, M. Sixt, and R. Voituriez, 2015. Actin Flows Mediate a Universal Coupling between Cell Speed and Cell Persistence. *Cell* 161:374–386. http://www.sciencedirect.com/science/article/pii/S0092867415001804.

52. Heyn, J. C. J., M. Atienza Juanatey, M. Falcke, and J. O. Rädler, 2025. Cell-mechanical parameter estimation from 1D cell trajectories using simulation-based inference. *PLoS One* 20:1–17. https://doi.org/10.1371/journal.pone.0310669.

53. Müller, P. M., J. Rademacher, R. D. Bagshaw, C. Wortmann, C. Barth, J. van Unen, K. M. Alp, G. Giudice, R. L. Eccles, L. E. Heinrich, et al., 2020. Systems analysis of RhoGEF and RhoGAP regulatory proteins reveals spatially organized RAC1 signalling from integrin adhesions. *Nat. Cell Biol.* 22:498–511.

54. Choi, C. K., M. Vicente-Manzanares, J. Zareno, L. A. Whitmore, A. Mogilner, and A. R. Horwitz, 2008. Actin and α-actinin orchestrate the assembly and maturation of nascent adhesions in a myosin II motor-independent manner. *Nat. Cell Biol.* 10:1039–1050.

55. Scales, T. M., and M. Parsons, 2011. Spatial and temporal regulation of integrin signalling during cell migration. *Curr. Opin. Cell Biol.* 23:562 – 568. http://www.sciencedirect.com/science/article/pii/S0955067411000810.

56. Sabra, H., M. Brunner, V. Mandati, B. Wehrle-Haller, D. Lallemand, A.-S. Ribba, G. Chevalier, P. Guardiola, M. R. Block, and D. Bouvard, 2017. 1 integrin–dependent Rac/group I PAK signaling mediates YAP activation of Yes-associated protein 1 (YAP1) via NF2/merlin. *J. Biol. Chem.* 292:19179–19197. https://www.sciencedirect.com/science/article/pii/S002192582032891X.

57. Böttcher, R. T., M. Veelders, P. Rombaut, J. Faix, M. Theodosiou, T. E. Stradal, K. Rottner, R. Zent, F. Herzog, and R. Fässler, 2017. Kindlin-2 recruits paxillin and Arp2/3 to promote membrane protrusions during initial cell spreading. *J. Cell Biol.* 216:3785–3798. https://doi.org/10.1083/jcb.201701176.

58. Welf, E. S., H. E. Johnson, J. M. Haugh, and A. Mogilner, 2013. Bidirectional coupling between integrin-mediated signaling and actomyosin mechanics explains matrix-dependent intermittency of leading-edge motility. *Mol. Biol. Cell* 24:3945–3955. https://www.molbiolcell.org/doi/abs/10.1091/mbc.e13-06-0311.

59. Jilkine, A., A. Marée, and L. Edelstein-Keshet, 2007. Mathematical Model for Spatial Segregation of the Rho-Family GTPases Based on Inhibitory Crosstalk. *Bull. Math. Biol.* 69:1943–1978. 10.1007/s11538-007-9200-6.

60. Hu, K., L. Ji, K. T. Applegate, G. Danuser, and C. M. Waterman-Storer, 2007. Differential transmission of actin motion within focal adhesions. *Science* 315:111–115.

61. Giannone, G., R.-M. Mège, and O. Thoumine, 2009. Multi-level molecular clutches in motile cell processes. *Trends Cell Biol.* 19:475–486.

Journal Pre-proof

62. Sabass, B., and U. S. Schwarz, 2010. Modeling cytoskeletal flow over adhesion sites: competition between stochastic bond dynamics and intracellular relaxation. *J. Phys.: Condens. Matter* 22:194112. https://doi.org/10.1088/0953-8984/22/19/194112.

63. Camley, B. A., Y. Zhao, B. Li, H. Levine, and W.-J. Rappel, 2013. Periodic Migration in a Physical Model of Cells on Micropatterns. *Phys. Rev. Lett.* 111:158102. https://link.aps.org/doi/10.1103/PhysRevLett.111.158102.

64. Evans, E., 2001. Probing the relation between force - lifetime - and chemistry in single molecular bonds. *Annu. Rev. Biophys. Biomol. Struct.* 30:105–128.

65. Evans, E. A., and D. A. Calderwood, 2007. Forces and Bond Dynamics in Cell Adhesion. *Science* 316:1148–1153. https://www.science.org/doi/abs/10.1126/science.1137592.

66. Allard, J., and A. Mogilner, 2013. Traveling waves in actin dynamics and cell motility. *Curr. Opin. Cell Biol.* 25:107–115.

67. Nayal, A., D. J. Webb, C. M. Brown, E. M. Schaefer, M. Vicente-Manzanares, and A. R. Horwitz, 2006. Paxillin phosphorylation at Ser273 localizes a GIT1–PIX–PAK complex and regulates adhesion and protrusion dynamics. *J. Cell Biol.* 173:587–589.

68. Smith, H. W., P. Marra, and C. J. Marshall, 2008. uPAR promotes formation of the p130Cas–Crk complex to activate Rac through DOCK180. *J. Cell Biol.* 182:777–790.

69. Edwards, D. C., L. C. Sanders, G. M. Bokoch, and G. N. Gill, 1999. Activation of LIM-kinase by Pak1 couples Rac/Cdc42 GTPase signalling to actin cytoskeletal dynamics. *Nat. Cell Biol.* 1:253–259.

70. Zheng, Y., S. Bagrodia, and R. A. Cerione, 1994. Activation of phosphoinositide 3-kinase activity by Cdc42Hs binding to p85. *J. Biol. Chem.* 269:18727–18730.

71. Higgs, H. N., and T. D. Pollard, 2001. Regulation of actin filament network formation through Arp2/3 complex: Activation by a Diverse Array of Proteins. *Annu. Rev. Biochem.* 70:649–676.

72. Ridley, A. J., M. A. Schwartz, K. Burridge, R. A. Firtel, M. H. Ginsberg, G. Borisy, J. T. Parsons, and A. R. Horwitz, 2003. Cell Migration: Integrating Signals from Front to Back. *Science* 302:1704–1709.

73. Mori, Y., A. Jilkine, and L. Edelstein-Keshet, 2008. Wave-Pinning and Cell Polarity from a Bistable Reaction-Diffusion System. *Biophys. J.* 94:3684–3697. https://www.sciencedirect.com/science/article/pii/S0006349508704442.

74. Eberhard, R. M., S. Kuhl, E. E. Celeboglu, G. Schwake, J. O. Rädler, and M. Falcke, in preparation. Protrusion Competition engenders Biphasic Relation between Cell Speed and Persistence Time of Cell Migration .

75. Erdmann, T., and U. S. Schwarz, 2004. Stochastic dynamics of adhesion clusters under shared constant force and with rebinding. *J. Chem. Phys.* 121:8997–9017. https://doi.org/10.1063/1.1805496.

76. Erdmann, T., and U. S. Schwarz, 2004. Stability of adhesion clusters under constant force. *Phys. Rev. Lett.* 92:108102.

77. van Kampen, N., 2001. Stochastic processes in physics and chemistry. North-Holland, Amsterdam.

78. Gardiner, C., 2009. Stochastic Methods. Springer Series in Synergetics. Springer Berlin, Heidelberg.

79. Yamashiro, S., H. Mizuno, M. B. Smith, G. L. Ryan, T. Kiuchi, D. Vavylonis, and N. Watanabe, 2014. New single-molecule speckle microscopy reveals modification of the retrograde actin flow by focal adhesions at nanometer scales. *Mol. Biol. Cell* 25:1010–1024. https://doi.org/10.1091/mbc.e13-03-0162, pMID: 24501425.

80. Wu, C., S. B. Asokan, M. E. Berginski, E. M. Haynes, N. E. Sharpless, J. D. Griffith, S. M. Gomez, and J. E. Bear, 2012. Arp2/3 complex is critical for lamellipodia and organization of cell-matrix adhesion but dispensable for fibroblast chemotaxis. *Cell* 148:973.

81. Deeg, J. A., I. Louban, D. Aydin, C. Selhuber-Unkel, H. Kessler, and J. P. Spatz, 2011. Impact of local versus global ligand density on cellular adhesion. *Nano Lett.* 11:1469–1476.

Journal Pre-proof

82. Pirone, D. M., W. F. Liu, S. A. Ruiz, L. Gao, S. Raghavan, C. A. Lemmon, L. H. Romer, and C. S. Chen, 2006. An inhibitory role for FAK in regulating proliferation: a link between limited adhesion and RhoA-ROCK signaling. *J. Cell Biol.* 174:277–288.

83. Pinto, V. I., V. W. Senini, Y. Wang, M. P. Kazembe, and C. A. McCulloch, 2014. Filamin A protects cells against force-induced apoptosis by stabilizing talin-and vinculin-containing cell adhesions. *FASEB J.* 28:453–463.

FIGURE 1

(A) The cell consists of two competing protrusions of lengths $L_{f,b}$ and the cell body. Front and back are coupled to the cell body by an effective elastic spring E. Polymerization forces $F_{f,b}$ push the membranes outward with velocities $v_{f,b}$ and lead to retrograde flow $v_{rf,b}$ of the F-actin network. This causes friction with coefficients $\kappa_{f,b}$ between the F-actin network and stationary structures in the cell (i.e. adhesions). During its movement, the cell experiences drag with coefficient ζ. (B) Actin polymerization at a rate v_e at the leading edge causes the membrane to move forward. This leads to the formation of nascent adhesions at a rate proportional to $k_v v_f \Theta(v_f)$ (or $k_v|v_b|\Theta(-v_b)$ at the trailing edge). Nascent adhesions disassemble or grow into larger focal adhesions at a rate proportional to k. The box symbolizes disassembled adhesion structures. Actin polymerization also creates a retrograde flow v_{rf}. The non-linear retrograde flow friction $\kappa_{f,b}$ can be described as a molecular clutch and is represented by the number of transient bonds between the F-actin network and adhesions. The bonds form and break with rates k_{on} and $k_{off}(v_r)$

FIGURE 2

(A-D) Bifurcation diagrams showing the friction coefficients $\kappa_{f,b}$ in dependence on ligand density B for different values of the parameter r. Full lines show stable stationary states and dotted lines unstable stationary states. Dashed lines indicate oscillatory behavior. Blue is used for the front friction coefficient, red for the back coefficient. The shaded regions show oscillation amplitudes of the moving oscillatory states. For the moving states the dashed lines indicate the maximum and minimum value of $\kappa_{f,b}$ during an oscillation. The amplitude of κ_f increases with r. We observe one stable state at low FN densities (SS). At the *branch point (BP)* (green dot) this state becomes unstable and two stable states emerge (MS up and down). Oscillatory states arise at the *Hopf bifurcation points* (green diamonds). (E-I) Example trajectories for the five morphodynamic states. Parameter set 1 was used for this simulations (see supplemental Table S1).

FIGURE 3

(A, C) Trajectories of two MDA-MB-231 cells in the MO2 state (A from (3), C from (50)). (B, D) Membrane velocities $v_{f,b}$ fo the cells in (A, B) over time. (E, G, I) Simulated trajectories starting in the three moving states MS (E), MO (G) and MO2 (I) without noise in bond formation and rupture. After 5 h of simulated time (dashed line), noise (Eq. 18) is turned on and all cells change into a noisy MO2 state showing that the moving states are excitable by noise. (F, H, J) Respective membrane velocities over time. Parameter set 1 was used for the simulations (see supplemental table T1).

FIGURE 4

(A) MO state for $r = 0$ at B = 80 ng/cm², (B) MO2 state for $r = 0.7$ at B = 80 ng/cm², (C) Weak and (D) strong perturbation of the back friction coefficient in the MS state at B = 35 ng/cm². Trajectories (top row), friction coefficients (second row), retrograde flow (third row) and membrane velocities (bottom row) over time. Weak perturbations affect the front membrane motion only slightly, which is similar to oscillations in the MO state (A, C). Strong perturbation significantly change the velocity of the front membrane, similar to oscillations in the MO2 state (B, D). Parameter set 1 was used for the simulations (see supplemental table T1).

FIGURE 5

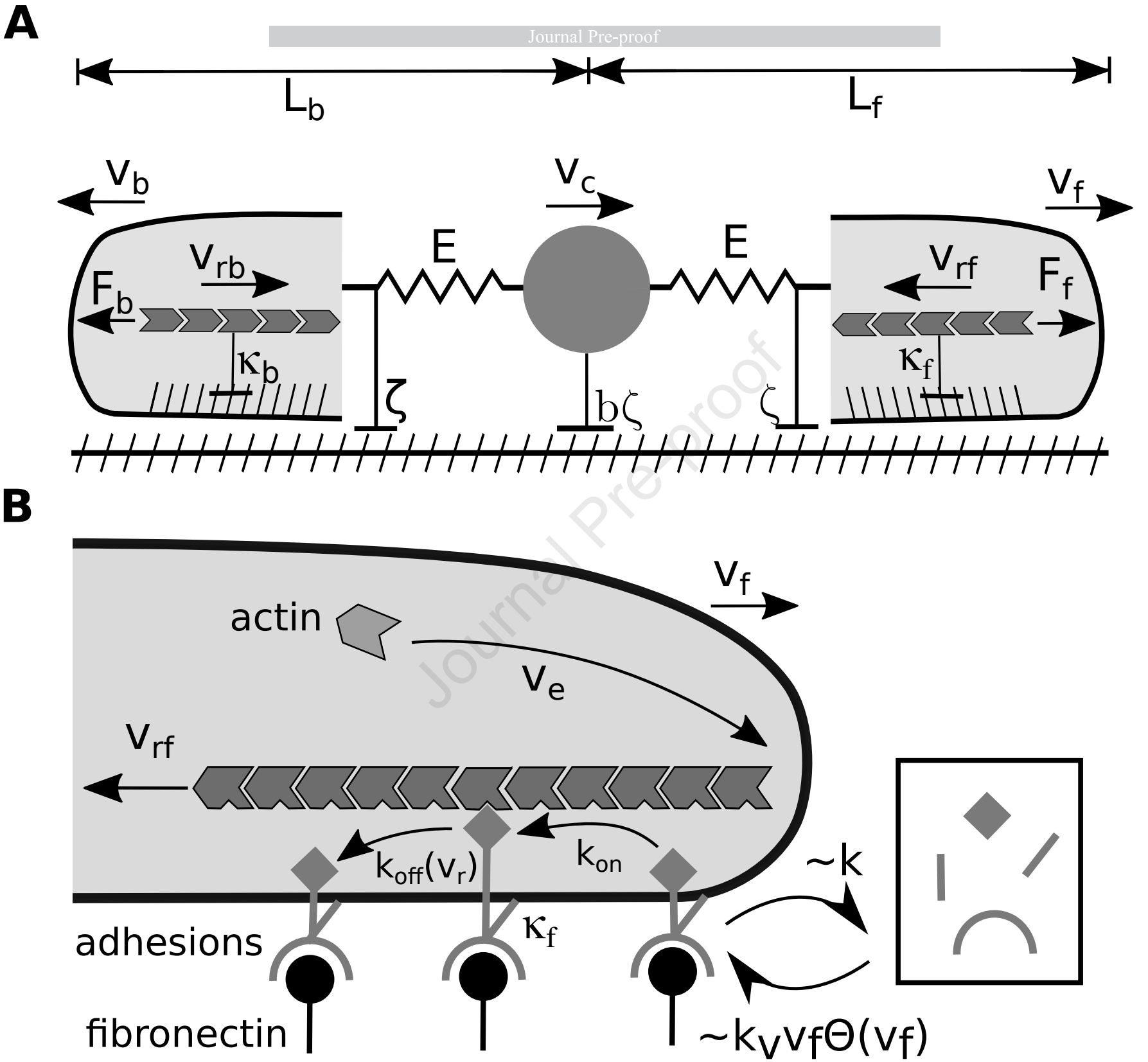
Biophysical model reproduces state distribution and state transition statistics of MDA-MB-231 cells. (A) Bifurcation diagram for the fitted model. Full lines show stable stationary states. Dashed lines indicate oscillatory behavior. Dotted lines represent unstable stationary and oscillatory states. Blue is used for the front friction coefficient, red for the back coefficient. The shaded regions show oscillation amplitudes of the moving oscillatory states. For the moving states the dashed lines indicate the maximum and minimum value of $\kappa_{f,b}$ during an oscillation. We observe one stable state at low FN densities (SS). At the *branch point (BP)* (green dot) this state becomes unstable and two stable states emerge (MS up and down). Oscillatory states arise at

Journal Pre-proof

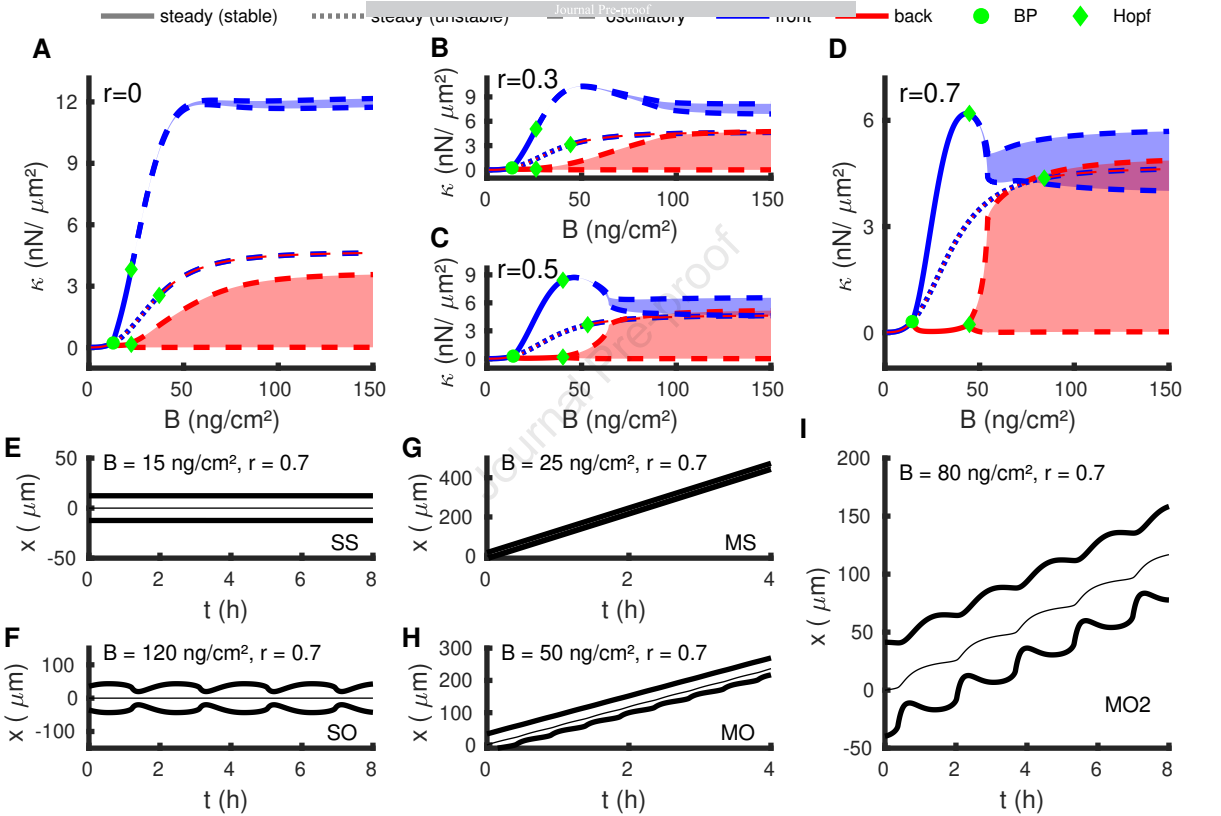
the *Hopf bifurcation points* (green diamonds) and MS states become unstable. At the next *Hopf bifurcation points* the MS states change their stability again. We also observe a fold bifurcation of limit cycles at the *limit point (LP)* (green star), were a stable and unstable limit cycle emerges, whereby the latter terminates at the second *Hopf bifurcation*. Thus, we have a bistability between MS and MO2 at high FN densities. (B) Fraction of measured time in each of the states and (C) state transition statistics for experimental and simulation data. Parameter set 2 was used for the simulations (see supplemental table T1).

Journal Pre-proof

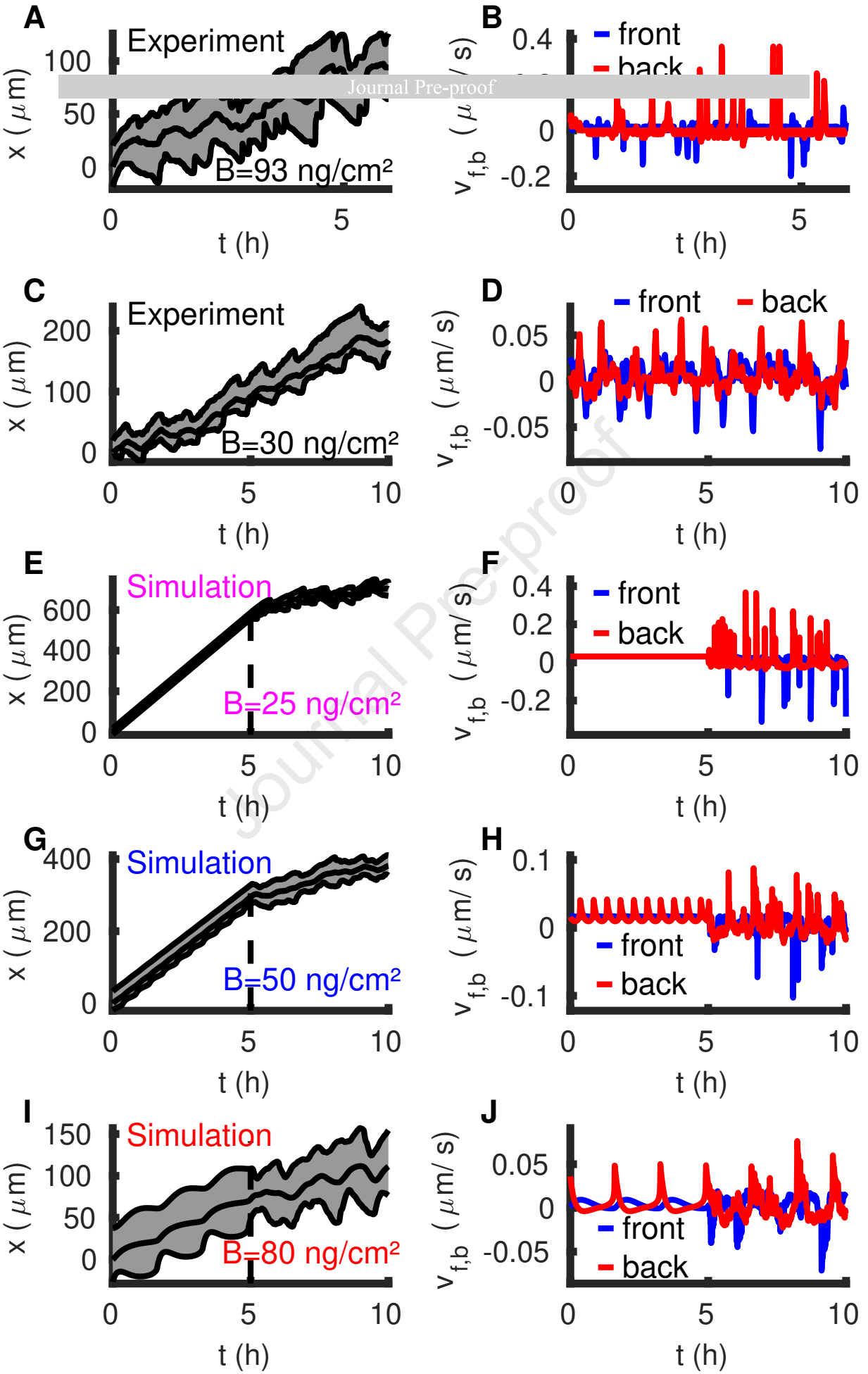
Journal Pre-proof

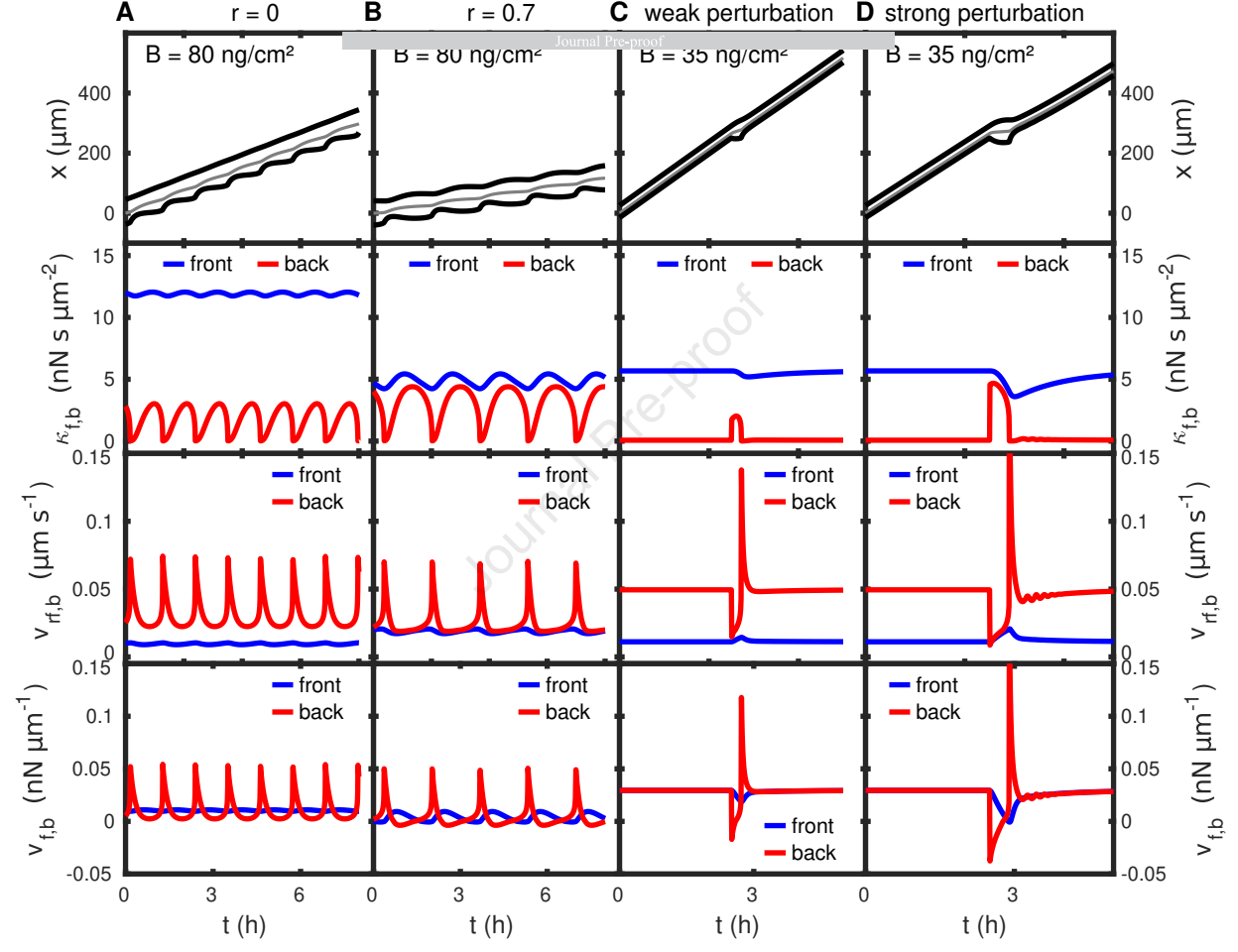


Journal Pre-proof



Journal Pre-proof




A
r = 0
B
r = 0.7
C
weak perturbation
D
strong perturbation
B = 80 ng/cm²
B = 80 ng/cm²
B = 35 ng/cm²
B = 35 ng/cm²
x (μm)
front
back
(nN s μm-2)
κf,b
vrf,b (μm s-1)
vf,b (nN μm-1)
t (h)
Journal Pre-proof

Journal Pre-proof

